IRAQI JOURNAL OF APPLIED PHYSICS
Vol. 22, No. 3, July-September 2026, pp. 433-440

Enhancement of Photoluminescence Characteristics of Dysprosium Ions in Ag-Dy^{3+} Co-doped PVA Network

Noor Alhuda H. Hashim [1]
Firas J. Kadhim [2]
Tabarak A. Al-Mashhadani [3*]

[1] College of Pharmacy, Uruk University, Baghdad, IRAQ
[2] Department of Physics, College of Science, University of Baghdad, Baghdad, IRAQ
[3] Institute of Laser for Postgraduate Studies, University of Baghdad, Baghdad, IRAQ
*Corresponding author Email: tabarak.amar1204a@sc.uobaghdad.edu.iq

In this study, Dy^{3+} doped and Ag- Dy^{3+} embedded Poly vinyl alcohol (PVA) host were synthesized at specific concentration of AgNPs and at different concentration of Dy^{3+}ions using chemical method. Spectroscopic analysis of silver nanoparticles in such polymer host revealed a distinct Surface Plasmon Resonance (SPR) band centered at 426 nm. Absorption and photoluminescence (PL) spectra of $DyCl_3.6H_2O$ in water solution were recorded at room temperature, as a function of Dy^{3+} concentration. Prominent emission bands from Dy^{3+} ions were observed at $^4F_{9/2} \rightarrow {}^6H_{13/2}$ and $^4F_{9/2} \rightarrow {}^6H_{15/2}$ under 350 nm excitation. The emission cross-section (σ_{em}) of the transtion $^4F_{9/2} \rightarrow {}^6H_{13/2}$ have been determined for doped and co-doped samples. PL analysis of co-doped PVA films demonstrated that the presence of silver nanoparticles significantly enhanced the PL intensity of Dy^{3+} ions. This enhancement is attributed to the strong local electric field generated by the SPR effect of metal nanoparticles. The Commission International del'Eclairage (CIE) chromaticity diagram has been used for investigating and observing white light emission, with all co-doped samples having color coordinates in the white range.

Keywords: Surface plasmon resonance; PVA; Photoluminescence, Emission cross-section
Received: 5 November 2025; Revised: 8 January 2026; Accepted: 15 January 2026; Published: 1 July 2026

1. Introduction

Organic luminescent materials doped with trivalent rare earth ions have recently been at the focus of much attention due to their potential applications within photonics, for instance, light-emitting diodes (LEDs), optical sensors, and display devices [1-3]. The basic physical properties of trivalent lanthanide ions have led to much attention being drawn to these fascinating materials, which consist of a general structure of a lanthanide and an organic matrix [4-7]. The fascinating optical properties associated with these materials are attributed to the characteristic intra-4f transitions, which cause a sharp band and emission and are weakly reliant on anions, as the 4f orbitals are shielded by the 5s and 5p orbitals. Host materials are essential when studying fine optical materials [8-11]. These materials exhibit good chromaticity and a high luminescence yield when activated by an appropriate wavelength. The photoluminescence (PL) observed in these materials occurs by the f–f or f–d transitions of Rare-Earth (RE) ions; the strength of the PL is dependent on the host matrix's composition and site symmetry [12-14]. Compared to other inorganic complexes, polymer-rare earth complexes offer additional benefits such transparency, superior mechanical qualities, simplicity of production, and design freedom [15]. Along with semi-crystal structure, polyvinyl alcohol (PVA), with various other advantages over other polymers like high mechanical strength, process ability, chemical resistance, solubility in water, high charge storage capacities, and high dielectric strength, is extensively used in the fields of contact lenses, synthetic fibers, paper production, textile materials, coatings, and binding agents [16-18]. Due to the absorption cross-section values close to zero, the emission efficiency for RE is very low. Various methods are being used by the scientific community to counter this restriction. The most effective method for increasing the emission efficiency of RE ions is embedding RE with metal NPs [19,20]. When metal NPs exhibit SPR or LSPR, the electric field around them is immensely enhanced. The process enhances the electric field of RE ions around the metal NPs. As such, the RE absorption cross section is effectively increased, which amplifies PL [21]. The application of such phenomena to RE-doped matrices has been helpful. The effect of LSPR depends prominently on the size, shape, spatial orientation, and coupling distance between the metal NPs and the RE ions along with the host dielectric [22-26]. The RE ions within a radius of 10 nm from the metal NPs feel an electric field that is stronger by a factor of approximately 100 compared to the incident field. This modifies the spectrum characteristics of the RE ions, increasing their excitation rates [27].

The trivalent dysprosium ion (Dy^{3+}), which has both blue and yellow emissions and intense luminescence in

a variety of lattices, is one of the greatest rare earth activators. These are necessary for the production of white light emission and are helpful in light emitting diodes (LEDs) and optical display systems. By adjusting the yellow-to-blue emission intensity ratio (Y/B), the total emission in the white light zone can be determined. The transition $^4F_{9/2} \rightarrow {}^6H_{15/2}$ is represented by the blue emission at 480 nm, the hypersensitive transition $^4F_{9/2} \rightarrow {}^6H_{13/2}$ ($D_J = 2$) by the yellow emission at 577 nm, and the transition $^4F_{9/2} \rightarrow {}^6H_{11/2}$ by the weak red emission at 670 nm. Generally speaking, Dy^{3+} exhibits three distinct emission bands [28].

The present study investigated the impact of the PVA host and Ag NPs on the photoluminescence characteristics of Dy^{3+} ions at different concentrations.

2. Experimental Part

5×10^{-3} mol/L as a specific concentration and 5 minutes as the reduction period after the boiling point were used to create the Ag colloids [29]. Dy^{3+} ions were obtained from Aldrich's 99.9% Dysprosium Chloride Hexahydrate ($DyCl_3.6H_2O$). 1.0×10^{-1} mol\L was obtained by dissolving 0.377 gm of $DyCl_3.6H_2O$ powder in deionized water to create various concentrations of Dy^{3+} solutions. A dilution was achieved to prepare other concentrations 2.0×10^{-2}, 35×10^{-3}, and 55×10^{-3} mol\L [30].

Ag:Dy^{3+} embedded PVA at a molecular weight of 10000 g/mol (BDH Chemicals, England) were prepared. 1.5 g of PVA powder was added into 10 mL of distilled water and let to swell for 24 hours at ambient temperature. 2 mL of both silver (Ag) colloids and $DyCl_3.6H_2O$ solution were added to the polymeric solution and stirred continuously during the entire process. The final solution was meticulously dispensed into flat glass plate dishes. The procedure was conducted multiple times using varying concentrations of Dy^{3+} solutions. Homogenous films were obtained following 36 hours drying period in an air oven at 40°C as illustrated in Fig. (1). The films thicknesses were measured and found to be in the range of 25±5μm.

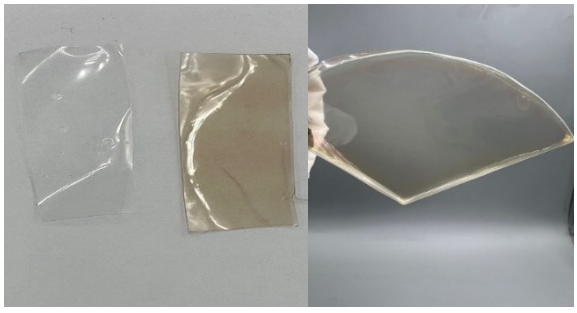

(a) (b) (c)

Fig. (1) Photos of (a) pure PVA film, (b) AgNPs-doped PVA film prepared specific concentration (5×10^{-3} M), (c) Ag-Dy^{3+} co-doped PVA film prepared at 0.0086% Dy^{3+} ions and at specific concentration (5×10^{-3} M) of AgNPs

3. Results and Discussions

In order to investigate the structural behavior of AgNPs within the PVA matrix, Fourier transform infrared (FTIR) spectrum was recorded for AgNPs doped PVA sample as shown in Fig. (2). The vibrational bands at around 3441.88, and 1639.43 cm^{-1} are ascribed to O–H starching and bending modes, while the bands at about 2905, 1639 and 1050 cm^{-1}, are assigned to C–H, C = C, and C-O stretching vibrations, respectively, for PVA [31] Moreover, vibration bands of AgNPs could arise at wavenumbers around 1018.16, 1364.39 and 1629.5 cm^{-1} [32]. These results give the primary impression that AgNPs do not have any links with the PVA network structure, and instead, they may tend to take positions within the structure as defects.

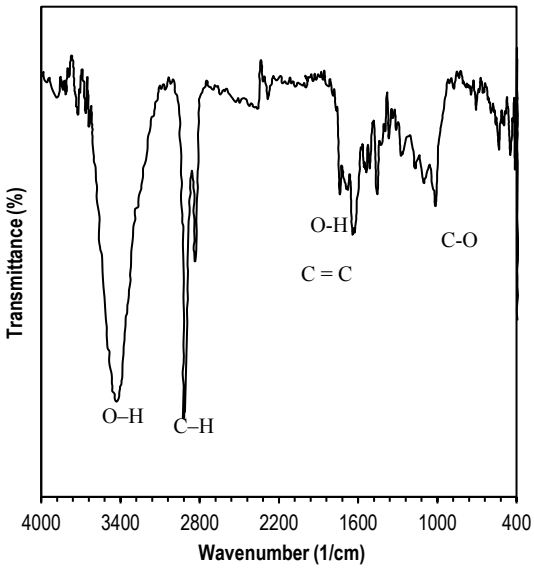

Fig. (2) FTIR spectrum of polymer embedded with AgNPs film

Figure (3) illustrates the X-ray diffraction (XRD) pattern of Ag-Dy^{3+} co-doped PVA film, acquired using a PHILIPS micro X-ray Diffractometer operating at PW1730. A distinct diffraction peak is noted at 2θ=20.25°, attributed to the semi-crystalline characteristics of the PVA polymer, resulting from robust intermolecular interactions among the PVA chains facilitated by hydrogen bonding between the molecules [33]. The crystallization of silver nanoparticles (AgNPs) has been revealed and it has been proven through the peak at 2θ = 37.9°, and was compared according to ASTM standards [34]. The average crystallite size of the AgNPs was estimated using the Scherrer's equation, yielding a value of approximately 7 nm, which confirms the nanoscale nature of the silver particles.

Figure (4) shows the obtained $DyCl_3$ solution's room-temperature absorption and photoluminescence spectra at different Dy^{3+} ion concentrations. Eight bands of Dy^{3+} ion absorption were observed at around 317, 352, 365, 374,446, 750, 810, and 911 nm. The 317 nm absorption band can be attributed to the

$^6H_{15/2}\rightarrow{}^4M_{17/2}$, $^6P_{3/2}$ transitions of Dy^{3+} ions. The bands at 352, 365 and 446 nm are related to the $^6H_{15/2}\rightarrow{}^4I_{13/2}$, $^4F_{7/2}$, $^6H_{15/2}\rightarrow{}^4M_{15/2}$, $^6P_{7/2}$ and $^6H_{15/2}\rightarrow{}^4I_{11/2}$ transitions of Dy^{3+} active sites, respectively. The 750, 810, and 911 nm bands are attributed to the $^6H_{15/2}\rightarrow{}^6F_{3/2}$, $^6H_{15/2}\rightarrow{}^6F_{5/2}$ and $^6H_{15/2}\rightarrow{}^6F_{7/2}$, transitions of Dy^{3+} active sites, respectively [35]. The excitation wavelength of 350 nm from a xenon lamp source in a Shimadzu RF-5301 PC Spectrofluorophotometer was used to obtained photoluminescence spectra. The spectra consist of two bands centered at around 485 nm and 581 nm which are attributed to the 4f-4f transitions; $^4F_{9/2}\rightarrow{}^6H_{15/2}$ and $^4F_{9/2}\rightarrow{}^6H_{13/2}$, respectively [36].

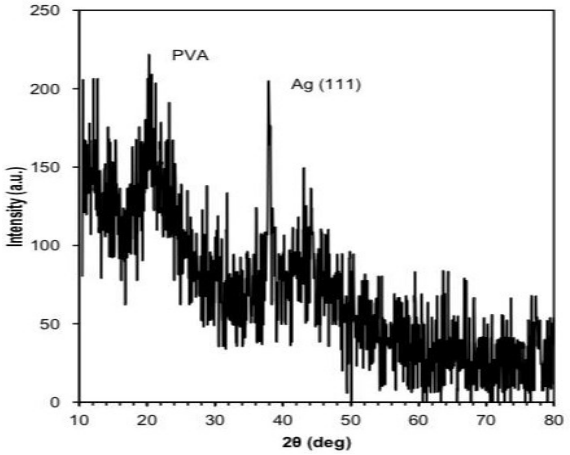

Fig. (3) XRD pattern of Ag-Dy^{3+} co-doped PVA film at 0.0086% Dy^{3+} ions and specific concentration (5×10^{-3} M) of AgNPs

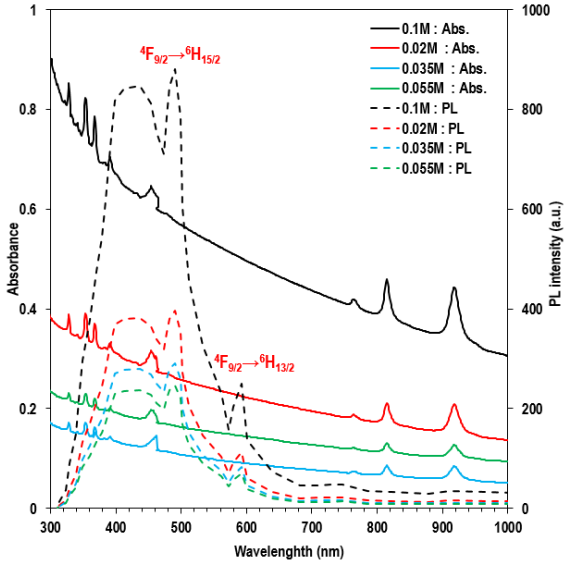

Fig. (4) The $DyCl_3$ solution's absorbance and PL spectra at different Dy^{3+} ion concentrations

Figure (5) shows the absorption spectra of different Dy^{3+} ions concentrations doped PVA films. Eight absorption bands that correspond to the intra configurational 4f-4f transitions of the Dy^{3+} ions are shown. According to the Beer- Lambert law, the absorbance increases as the concentration of Dy^{3+} increases, this is because the ions' contribution to the absorption process increases too [37]. The absorption spectra of Dy^{3+}-doped films show slight shifts and band broadening due to the influence of the PVA host matrix, which modifies the local environment around the ions and affects oscillator strengths [38,39].

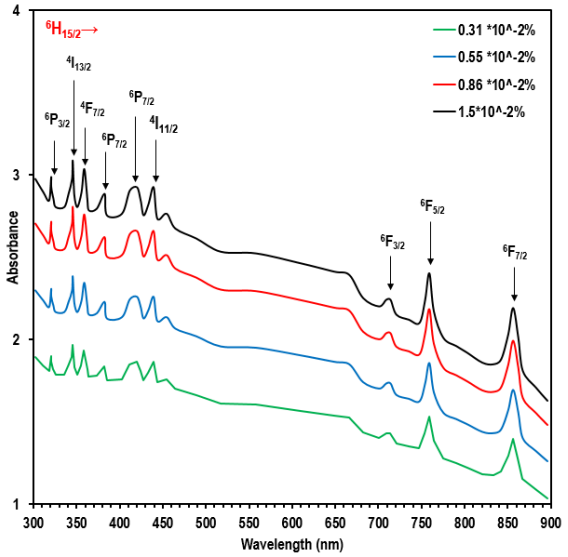

Fig. (5) The absorption spectra of different concentrations Dy^{3+} doped PVA films

On the other side and for the same set of samples, the photoluminescence spectra of Dy^{3+} doped PVA films at different concentrations of Dy^{3+} ions are shown in Fig. (6). The emission bands at 575 nm and 482 nm are caused by the transitions $^4F_{9/2}\rightarrow{}^6H_{13/2}$ and $^4F_{9/2}\rightarrow{}^6H_{15/2}$, while the band at $^4F_{9/2}\rightarrow{}^6H_{13/2}$ a hypersensitive induced electric dipole transition with $\Delta J = \pm2$ and $\Delta L = \pm2$ is associated with emission in the yellow region, where the host environment performs an essential part, the band at $^4F_{9/2}\rightarrow{}^6H_{15/2}$ in the blue region is known to be host insensitive and ($\Delta J = 0, \pm1$ but $0 \rightarrow 0$ banned) corresponds to the magnetic dipole. The emission intensity of the sample with a Dy^{3+} concentration of 0.0086% was higher than that of the other samples, which is significant. High doping levels for Dy^{3+} ions produce luminescence quenching, which increases the likelihood of non-radiative energy transfer processes including dipole-dipole interactions and cross-relaxation, this phenomenon is caused by an increase in non-radiative decay channels [40].

The absorption spectra of Ag-Dy^{3+} co-doped PVA films at different concentrations of Dy^{3+} ions and at specific AgNPs concentration of 5×10^{-3} M are shown in Fig. (7). Each spectra comprises eight absorption bands, one of which corresponds to the SPR of AgNPs at 426 nm and the other to the Dy^{3+} ions' intra-configuration 4f-4f transitions [41]. These bands' existence in Ag-Dy^{3+} co-doped PVA films is a sign of the ions' spectroscopic activity [42].

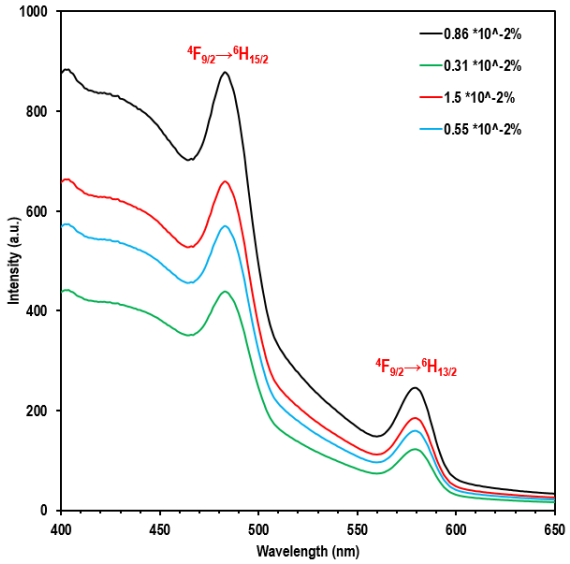

Fig. (6) The PL spectra of Dy^{3+} doped PVA films at different concentrations of Dy^{3+} ions

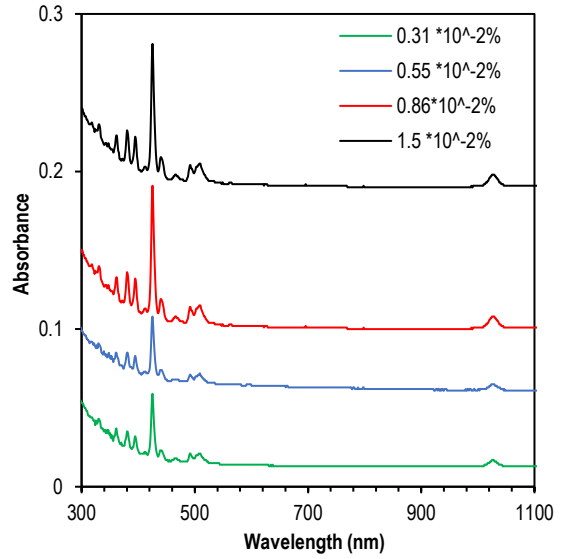

Fig. (7) The absorption spectra of Ag- Dy^{3+} co-doped PVA films at specific concentration (5×10^{-3} M) of AgNPs and different concentrations of Dy^{3+} ions

Photoluminescence spectra of the Ag-Dy^{3+} co-doped PVA films in Fig. (8) were obtained by excitation at a wavelength of 350 nm. It is evident that the monoliths' PL intensity has grown. A possible explanation for this could be the local field effect (LFE) caused by the SPR of metallic nanoparticles. SPR polaritons are created by an oscillation of electrons moving across the surface of metal nanoparticles due to the difference in permittivity between the metal and the host [43]. Due to these oscillations, a restricted electromagnetic field is created near the nanoparticles, increasing the local electric field surrounding them [44].

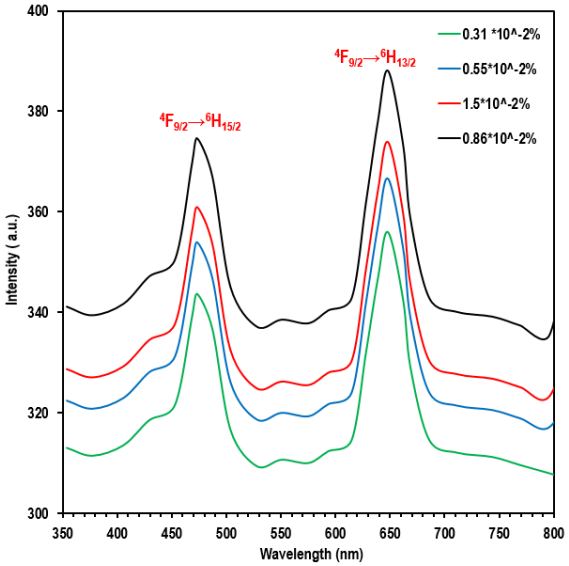

Fig. (8) The PL spectra of Ag-Dy^{3+} co-doped PVA films at specific concentration (5×10^{-3} M) of AgNPs and different concentrations of Dy^{3+} ions

The calculated spectroscopic parameter, for the transition from the Dy^{3+} ion emission band $^4F_{9/2}\rightarrow{}^6H_{13/2}$, is shown in table (1). The photoluminescence (PL) of PVA nanocomposites doped with Dy^{3+} ions and co-doped with Ag nanoparticles was analyzed in terms of radiative lifetime (τ_{rad}), fluorescence lifetime (τ_f), quantum efficiency (q_f), and emission cross-section (σ_{em}). For Dy^{3+}-doped PVA, τ_{rad} and τ_f show a non-monotonic dependence on Dy^{3+} concentration, mainly due to concentration quenching from Dy^{3+}-Dy^{3+} interactions, which enhance non-radiative energy transfer and multiphonon relaxation in the hydroxyl-rich polymer matrix [45]. In contrast, co-doping with Ag nanoparticles markedly improves PL performance, as evidenced by increased q_f, τ_f, and σ_{em} [46]. The emission cross-section was calculated using the Füchtbauer–Ladenburg equation (Eq. 1), which has been widely applied in rare-earth-doped systems to accurately estimate radiative emission properties [47].

$$\sigma_p = \lambda_p^4 / 8\,\pi\,\acute{n}^2\,\Delta\lambda_{eff.}\,\tau_{rad} \qquad (1)$$

where λ_p is the peak wavelength within the fluorescence band, $\Delta\lambda_{eff.}$ is the fluorescence linewidth (effective)

From the association between peak emission cross-section (σ_{em}) and Dy^{3+} concentrations, it is evident that the σ_{em} begins to increase with the concentration of Dy^{3+} ions, to a maximum value of 0.0086% (Fig. 9). As the concentration of Dy^{3+} ions increase, the σ_{em} decreases. This behavior is caused at high doping levels, the concentration quenching and luminesces quenching related to the O-H vibrations of water, for the co-doped samples, σ_{em} increases as the concentration of Dy^{3+} ions increases [48]. At higher Dy^{3+} concentrations, the reduced interionic distance enhances dipole–dipole interactions and promotes

cross-relaxation processes between neighboring Dy^{3+} ions. According to Dexter-type energy transfer mechanisms, these interactions introduce efficient non-radiative decay pathways, leading to concentration quenching and a decrease in the emission intensity. The observed photoluminescence enhancement in Ag- Dy^{3+} co-doped PVA is primarily due to plasmon-induced local electric field amplification and radiative coupling effects [49].

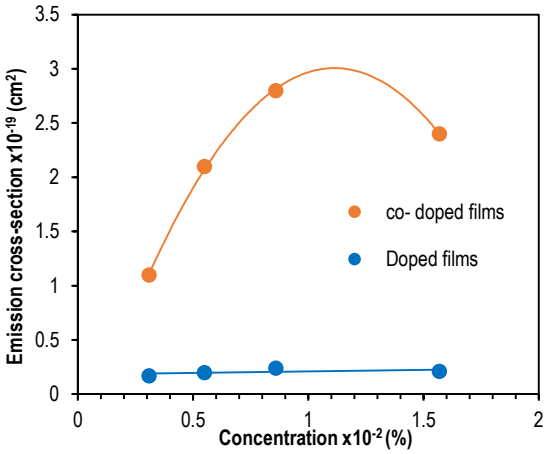

Fig. (9) Peak emission cross-section (σ_{em}) in doped and co-doped films varies with Dy^{3+} ion concentrations

The oscillator strength analysis of Ag-Dy^{3+} co-doped PVA films shows excellent agreement between experimental (f_{exp}) and calculated (f_{cal}) values, with deviations ranging from 0.13×10^{-6} to 0.24×10^{-6}, indicating a high-quality fit of the Judd–Ofelt theoretical model to the experimental absorption data is shown in table (2) [50]. Among the electronic transitions, $^6H_{15/2}\rightarrow{}^6P_{7/2}$ (λ=365nm) exhibits the highest oscillator strength, reflecting a significant probability for electric-dipole transitions, followed by $^6H_{15/2}\rightarrow{}^4I_{11/2}$, and $^6H_{15/2}\rightarrow{}^6F_{3/2}$ with gradually decreasing strengths, consistent with selection rules and the multiples structure of Dy^{3+}.

The enhancement in the photoluminescence properties can be further correlated with Judd–Ofelt intensity parameters (Ω_2, Ω_4, Ω_6) is shown in table (2). The relatively high Ω_2 values indicate increased asymmetry and covalence around Dy^{3+} ions due to coordination with hydroxyl groups of PVA and the presence of Ag nanoparticles. This enhanced asymmetry leads to stronger electric-dipole transitions, particularly for the hypersensitive transitions of Dy^{3+} [51].

The photo of the co-doped sample's luminescence at 350 nm using a diode laser source at 0.0086% concentrations of Dy^{3+} ions is shown in Fig. (10a). All of the work's earlier findings suggest that doped materials have the ability to produce white light when combined with a UV light source, this ability is enhanced when silver nanoparticles are present [52].

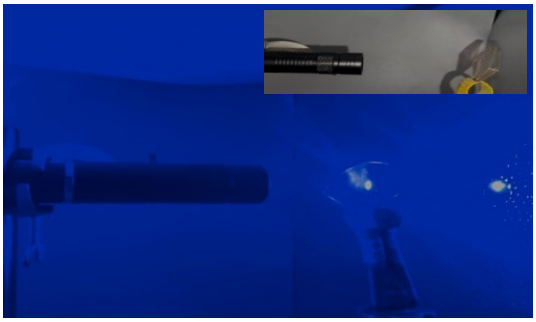

(a)

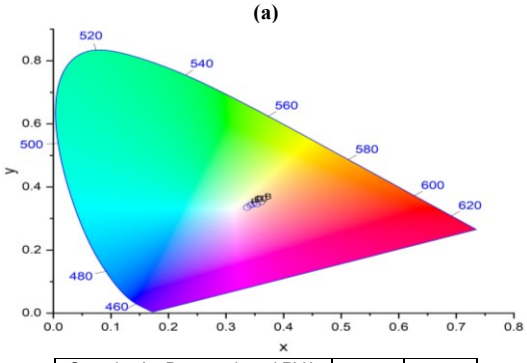

Sample: Ag-Dy^{3+} co-doped PVA	x	y
Ag-Dy^{3+}	0.346	0.344

(b)

Fig. (10) Ag-Dy^{3+} co-doped PVA films at 0.0086% Dy^{3+} ions concentrations and specific concentration of AgNPs 5×10^{-3} M excited at 350 nm; (a) The photoluminescence photograph using a diode laser source (b) Chromaticity diagram

According to the chromaticity diagram for International deI'Eclairage (CIE) (Fig. 10b), the Ag-Dy^{3+} co-doped PVA films were determined as **x=0.346** and **y=0.344**. Using the McCamy approximation, the correlated color temperature (CCT) is calculated to be approximately **6150 K**, indicating daylight white emission [53]. The estimated color-rendering index (CRI) is in the range of **92–95**, reflecting high-quality white light. The measured white point is slightly warm and moderately shifted toward the yellow region compared to the ideal white point (0.333, 0.333) [53].

The yellow-to-blue emission ratio (Y/B) for the Ag–Dy^{3+} co-doped PVA sample was estimated to be approximately **1.11**, indicating a slight dominance of the yellow component over blue. This is consistent with the observed warm white emission. The sample's position on the CIE 1931 chromaticity diagram, highlighting the Y/B ratio visually. This slight shift is consistent with previous studies reporting that minor variations in the host matrix composition or dopant concentration can influence the chromaticity coordinates and CCT of rare-earth-doped polymer films [54].

4. Conclusions

In this study, Dy^{3+}-AgNPs co-doped PVA films exhibited high transparency and thermal stability, along with a pronounced enhancement in photoluminescence

intensity, mainly attributed to the localized electric field generated by the surface plasmon resonance of Ag nanoparticles, which strengthens the radiative transitions of Dy^{3+} ions located within the plasmonic near-field region. At elevated Dy doping levels, the reduced interionic distance promotes diople-dipole interactions and cross-relaxation processes among Dy ions, as described by Dexter-type energy transfer mechanisms. These processes facilitate non- radiative decay pathways, leading to a reduction in emission intensity. These findings confirm that Dy^{3+}/AgNPs co-doped PVA films represent a promising platform for white-light applications.

References

[1] K.N. Kumar et al., "Bright green emission from f-MWCNT embedded co-doped Bi^{3+}/Tb^{3+}:Polyvinyl alcohol polymer nanocomposites for photonic applications", *RSC Adv.*, 7(25) (2017) 15084-15095.

[2] L. Xia et al., "Temperature/electric field induced photoluminescence-modulation effect in dysprosium-doped barium titanate ferroelectric ceramics", *J. Materiomics*, 10(5) (2024) 1117-1125.

[3] P.N.K. Chaitanya et al., "Structural and luminescent properties of Dy^{3+}-doped Ca_3WO_6 phosphors for white-light display applications", *RSC Adv.*, 15(25) (2025) 19872-19883.

[4] F. Kang et al., "Recent advances and prospects of persistent luminescent materials as inner secondary self-luminous light source for photocatalytic applications", *Chem. Eng. J.*, 403 (2021) 126099.

[5] N.T. Hien et al., "Optical properties and Judd–Ofelt analysis of Dy^{3+} doped $CoAl_2O_4$ nanocrystals", *Nanoscale Adv.*, 6(22) (2024) 5598-5611.

[6] Y. Bi et al., "Thermostability and photoluminescence of Dy(iii) single-molecule magnets under a magnetic field", *Chem. Sci.*, 7(8) (2016) 5020-5031.

[7] M. Sheoran et al., "Fabrication and photoluminescent features of cool-white light emanating Dy^{3+} doped $Ba_5Zn_4Gd_8O_{21}$ nanophosphors for near UV-excited pc-WLEDs", *Chem. Phys. Impact*, 4 (2022) 100063.

[8] J.-C.G. Bünzli and S.V. Eliseeva, "Lanthanide luminescence for functional materials and bio-sciences", *Chem. Soc. Rev.*, 39 (2010) 189-227.

[9] A.P. Tejas et al., "Temperature-responsive dual-emission $Ba_2ZnSi_2O_7$ phosphors co-doped with Tb^{3+} and Dy^{3+} for optical thermometry applications", *J. Sci.: Adv. Mater. Dev.*, 10(4) (2025) 101054.

[10] S. Krishnaswamy et al., "Investigation of the optical properties of Dy doped ZnO/PVA thin film: White light emission for LED application", *Result. Opt.*, 18 (2025) 100786.

[11] S. Gouraha et al., "Enhanced photoluminescence and photocatalytic properties in Dy-doped sodium zinc molybdate synthesized via a green microwave-assisted method", *Nanoscale Adv.*, 7(10) (2025) 3038-3048.

[12] B. Zheng et al., "Rare-earth doping in nanostructured inorganic materials", *Chem. Rev.*, 122(6) (2022) 5519-5603.

[13] A.N. Sahu et al., "White light emission from Eu, Dy doped $NaCa(PO_3)_3$ phosphor for WLED applications", *Next Mater.*, 9 (2025) 101169.

[14] R.V. Tikale, A.R. Kadam and S.J. Dhoble, "Synthesis and optical properties of $LiZr_2(PO_4)_3:Eu^{3+}$, Dy^{3+} phosphor for display devices application", *Chem. Phys. Impact*, 8 (2024) 100525.

[15] M.O. Reddy and B.C. Babu, "Structural, optical, electrical, and magnetic properties of PVA:Gd^{3+} and PVA:Ho^{3+} polymer films", *Indian J. Mater. Sci.*, (2015), article ID 927364, https://doi.org/10.1155/2015/927364

[16] A. Soylu, O. Karaahmet and B. Cicek, "Exploring luminescence in transparent glass–ceramic coating: Study on Pr^{3+}/Dy^{3+} co-doped SrO–Al_2O_3–SiO_2 glass–ceramic particles", *Mater. Chem. Phys.*, 318 (2024) 129250.

[17] K.A. Rathi et al., "Influence of La^{3+} co-doping on the photoluminescence properties of YAG:Dy^{3+} electrospun light emitting nanofibers", *Result. Opt.*, 12 (2023) 100492.

[18] A.N. Yerpude et al., "Synthesis and photoluminescence characteristics of $Ba_2Ca(PO_4)_4:Dy^{3+}$ phosphors for n-UV based solid-state lighting", *Mater. Lett. X*, 18 (2023) 100196.

[19] N. Shasmal and B. Karmakar, "Tuneable and Au-enhanced yellow emission in Dy^{3+}/Au co-doped antimony oxide glass nanocomposites", *J. Non-Cryst. Solids*, 463 (2017) 40-49.

[20] B.-G. Zhai, M.M. Chen and Y.M. Huang, "Photoluminescence and afterglow of Dy^{3+} doped $CaAl_2O_4$ derived via sol–gel combustion", *RSC Adv.*, 12(49) (2022) 31757-31768.

[21] T.A. Al-Mashhadani et al., "Biochemical effects of silver nanoparticles prepared by chemical reduction method on male rat kidney functions and antioxidant defense systems", *Agric. Sci. Digest*, 1 (2024) 1-7.

[22] A. Kumar et al., "Physical, structural and optical characterization of Dy^{3+} doped ZnF_2–WO_2–B_2O_3–TeO_2 glasses for opto-communication applications", *Opt. Mater.*, 114 (2021) 110937.

[23] M. Thangaraj et al., "Enhanced reddish-orange luminescence from Sm^{3+}/Ag co-doped barium zinc borophosphate glasses: Structural and Judd–

Ofelt analysis", *J. Non-Cryst. Solids*, 625 (2024) 122752.
[24] N. Dehingia et al., "Effect of Ag nanoparticles on the Judd–Ofelt and radiative parameters of Sm^{3+} ions in sol–gel silica matrix", *J. Lumin.*, 226 (2020) 117414.
[25] T.A. Al-Mashhadani, F.J. Kadhim and N.A.H. Hashim, "Optimization of surface plasmon resonance band of copper nanoparticles doping in silica xerogels", *Iraqi J. Appl. Phys.*, 20(2B) (2024) 465-468.
[26] V.L. Paperny et al., "Enhancement of photoluminescence from rare-earth ions in fluoride crystals by ion-implanted silver nanoparticles", *J. Lumin.*, 279 (2025) 121044.
[27] A. Kumar and J. Manam, "Color tunable emission and temperature-dependent photoluminescence properties of Eu^{3+} co-doped $Gd_2Zr_2O_7$:Dy^{3+} phosphors", *Opt. Mater.*, 96 (2019) 109373.
[28] S.K. Gupta et al., "Photoluminescence investigations of the near white light emitting perovskite ceramic $SrZrO_3$:Dy^{3+} prepared via gel-combustion route", *Int. J. Appl. Ceram. Technol.*, 10(4) (2013) 593-602.
[29] T.A. Al-Mashhadani and F.J. Al-Maliki, "Optimized characteristics of silver nanoparticles synthesized by chemical reduction and embedded in silica xerogels", *Iraqi J. Appl. Phys.*, 18(3) (2022) 1-7.
[30] T.A. Al-Mashhadani and F.J. Kadhim, "Photoluminescence properties of silver–dysprosium co-doped silica obtained by sol–gel method", *J. Sol-Gel Sci. Technol.*, 106(2) (2023) 553-560.
[31] P.H. Scudder, **"Electron flow in organic chemistry: A decision-based guide to organic mechanisms",** John Wiley & Sons (2023).
[32] S. Marimuthu et al., "Evaluation of green synthesized silver nanoparticles against parasites", *Parasitol. Res.*, 108 (2011) 1541-1549.
[33] A. Bouzidi et al., "Simple synthesis and characterization of novel polyvinyl alcohol capped sodium selenite solid composite film (PVA:NaSe SCF) samples", *J. Sci.: Adv. Mater. Dev.*, 7(3) (2022) 100458.
[34] X. Hong et al., "Dry-wet spinning of PVA fiber with high strength and high Young's modulus", *IOP Conf. Ser.: Mater. Sci. Eng.*, 439(4) (2018) 042011.
[35] S. Hamdi et al., "Enhancing the structural, optical and electrical conductivity properties of ZnO nanopowders through Dy doping", *Inorg. Chem. Commun.*, 144 (2022) 109819.
[36] P. Sehrawat et al., "Emanating cool white light emission from novel down-converted $SrLaAlO_4$: Dy^{3+} nanophosphors for advanced optoelectronic applications", *Ceram. Int.*, 46(10) (2020) 16274-16284.
[37] G. Chen et al., "Upconversion nanoparticles: design, nanochemistry, and applications in theranostics", *Chem. Rev.*, 120(5) (2020) 2536-2591.
[38] X. Li, J. Song and Y. Wang, "Plasmonic enhancement of lanthanide-doped nanomaterials: mechanisms, characterization, and applications", *Adv. Opt. Mater.*, 9(2) (2021) 2001345.
[39] M.A. Marzouk and S.M. Abo-Naf, "Structure characterization and photoluminescence of sol-gel synthesized Ag-Dy-co doped silica phosphor", *J. Non-Cryst. Solids*, 505 (2019) 292-300.
[40] V. Sharma, S. Maurya and A.S. Rao, "Photoluminescence and optical studies of a temperature sustainable Dy^{3+} doped silicate phosphor for photonic applications", in *Int. Conf. Adv. Funct. Mater. Devices*, Springer Nature (Singapore, 2023), pp. 1-10.
[41] A. U. Ahmad et al., "Amplified optical response of Dy^{3+}-activated lithium-strontium-zinc-borate glasses: Role of Ag nanoparticles concentration changes", *J. Non-Cryst. Solids*, 610 (2023) 122287.
[42] L. Cherupally, "Influence of rare Earth doping and modifier oxides on optical and thermoluminescence properties of tellurite glasses for radiation dosimetry applications", *East Afr. J. Sci. Technol. Innov.*, 6 (2024) 1-12.
[43] S.S. Al-Awadi, R.T. Shbeeb and B.T. Chiad, "Effect of silver nanoparticles on fluorescence spectra of C480 dye", *Iraqi J. Sci.*, 59(1C) (2018) 502-509.
[44] S. Das and R. Sharma, "Localized surface plasmon resonance assisted enhancement of Dy^{3+} emission in polymer hosts", *Opt. Mater.*, 108 (2020) 110450.
[45] A. Kumar, V. Singh and S.B. Rai, "Plasmon-enhanced luminescence in rare-earth-doped polymer nanocomposites", *J. Lumin.*, 206 (2019) 1-10.
[46] I. Couwenberg et al., "Spectroscopic properties of the trivalent terbium ion in the huntite matrix $TbAl_3(BO_3)_4$", *J. Alloys Compd.*, 274(1-2) (1998) 157-163.
[47] B.R. Judd, "Optical absorption intensities of rare-earth ions", *Phys. Rev.*, 127(3) (1962) 750-761.
[48] M. Rai, S. Ghosh and S. Das, "Plasmon–rare earth ion interactions in Ag nanoparticle-doped luminescent materials", *Prog. Mater. Sci.*, 114 (2020) 100686.
[49] G.S. Ofelt, "Intensities of crystal spectra of rare-earth ions", *J. Chem. Phys.*, 37(3) (1962) 511-520.
[50] W.A. Pisarski, "Judd–Ofelt Analysis and Emission Properties of Dy^{3+} Ions in Borogermanate Glasses", *Materials,* 15 (2022) 9042.
[51] J. A. Jiménez et al., "Insights into the structural, thermal/dilatometric, and optical properties of

Dy^{3+}-doped phosphate glasses for lighting applications", *ACS Phys. Chem. Au*, 4(6) (2024) 720-735.

[52] E. V. Salerno et al., "Tuning white light emission using single-component tetrachroic Dy^{3+} metallacrowns: the role of chromophoric building blocks", *Chem. Sci.*, 15(21) (2024) 8019-8030.

[53] A.K. Guria, B.K. Patra and M.M. Sk, "Emerging new- generation colloidal halide perovskite nanocrystals with white photoluminescence", *ChemNanoMat*, 11(4) (2025) e202500021. https://doi.org/10.1002/cnma.202500021

[54] L. Huang et al., "Fixed Yellow-to-Blue Intensity Ratio of Dy^{3+} in $KY(CO_3)_2$ Host for Emission Color Tuning", *Materials (Basel)*, 17(6) (2024) 1438.

Table (1) The PVA films doped with Dy^{3+} ions and co-doped with Ag-Dy^{3+} ions spectroscopic parameters

Dy^{3+} ions concentration $\times10^{-2}$ (%)	Doped films				Co-doped films			
	τ_{rad} (ms)	q_f	τ_f (ms)	$\sigma_{em} \times 10^{-19}$ (cm^2)	τ_{rad} (ms)	q_f	τ_f (ms)	$\sigma_{em} \times 10^{-19}$ (cm^2)
1.5	1.54	0.027	0.040	0.21	1.23	0.158	0.194	2.4
0.86	1.36	0.031	0.042	0.24	1.05	0.301	0.316	2.8
0.55	1.63	0.023	0.038	0.20	1.40	0.411	0.575	2.1
0.31	1.92	0.037	0.071	0.17	2.67	0.973	2.59	1.1

Table (2) Oscillator strengths and Judd–Ofelt parameters of Ag–Dy^{3+} co-doped PVA films

Parameter	$^6H_{15/2}\rightarrow{}^6P_{7/2}$	$^6H_{15/2}\rightarrow{}^4I_{11/2}$	$^6H_{15/2}\rightarrow{}^6F_{3/2}$
Wavelength, λ (nm)	365	446	750
f_{exp} ($\times10^{-6}$)	7.42	5.81	3.12
f_{cal} ($\times10^{-6}$) [36]	7.18	5.96	3.25
$\Delta f = \lvert f_{exp} - f_{cal}\rvert$ ($\times10^{-6}$)	0.24	0.15	0.13
Ω_2 ($\times10^{-20}$ cm^2)	6.12		
Ω_4 ($\times10^{-20}$ cm^2)	2.48		
Ω_6 ($\times10^{-20}$ cm^2)	1.03		
Typical range ($\times10^{-20}$ cm^2) [37]	Ω_2: 5–7, Ω_4: 2–3, Ω_6: 1–2		
Interpretation	$\Omega_2 > \Omega_4 > \Omega_6$ indicates enhanced asymmetry and covalent character around Dy^{3+} ions		

